

Superluminal Motions of AGNs and GRBs at Multiple-Frequencies

Zhi-Bin Zhang^{1,2}

¹ Department of Physics, College of Physics, Guizhou University, Guiyang, Guizhou 550025, China.
e-mail: zbzhang@gzu.edu.cn

² College of Physics and Engineering, Qufu Normal University, Qufu 273165, China.

Preprint online version: August 29, 2018

ABSTRACT

Context. Superluminal motion has been found to occur in many kinds of celestial bodies with the relativistic ejecta, especially for some active galactic nuclei (AGNs), gamma-ray bursts (GRBs) and micro-quasars, although these objects are largely different in their lifetimes, sizes and features.

Aims. To investigate the discrepancy in above inhomogeneous objects, we have compared the apparent superluminal motion of GRBs with AGNs, both of them being cosmological outbursts. In addition, properties of the superluminal motion between different subclasses of AGNs (e.g., Radio galaxies, BL Lac objects, and Quasars) are also compared in detail. Particularly, we focus on two low luminosity GRBs, namely 060218 and 170817A, that are ultra-long and short bursts associated with supernova and gravitational wave respectively.

Methods. For these, statistical methods including linear regression analysis, linear correlation and K-S test have been used. Antitheses and theoretical analysis of models are also adopted to contrast between AGNs and GRBs, as well as their individual subgroups at aspect of theory and observation.

Results. The apparent transverse velocity (β_{app}) of Swift and pre-Swift GRBs are tightly correlated with the Doppler factor δ as $\beta_{app} \propto \delta^{0.5}$, while all AGNs distribute around the line of $\beta_{app} = \delta$ behaving a weak correlation of β_{app} with δ . In contrast, β_{app} is positively correlated with Lorentz factor (γ) or $\gamma^2(1+z)^{-1}$, not for GRBs but for AGNs. β_{app} and $1+z$ are independent for neither GRBs nor AGNs, but apparently exhibit a positive correlation of β_{app} with $1+z$ from AGNs to GRBs, showing a cosmological effect of evolution with redshift. I also found that GRB 170817A and GRB 060218 are outliers of the above correlations.

Conclusions. Superluminal properties of GRBs are significantly different from those of AGNs. However, there are no obvious differences between radio galaxies, BL Lac objects, and quasars in terms of their superluminal motion. In despite of radiation mechanism, beaming effect and cosmological expanding would play the same roles on the superluminal motion for AGNs and GRBs.

Key words. gamma-ray bursts–active galactic nuclei–apparent superluminal motion–cosmology

1. Introduction

The apparent superluminal phenomenon was first predicted by Rees (1966) that the transverse velocity of an object moving (ultra-)relativistically in some special directions may appear to exceed the speed of light. At first glance such a motion is quite counter-intuitive, whereas it does not violate the special relativity. It is essentially a geometric effect or a light travel-time effect in the frame of standard model (Chodorowski 2005).

This motion is initially confirmed and discovered by using new technique of spectroscopy called as very long baseline interferometry (VLBI) for radio galaxies and quasars (Whitney et al. 1971, Cohen et al. 1971). So far, it has been known that the superluminal motion is not unique to quasars and radio galaxies, but also to other sources including micro-quasars and BL Lac objects (e.g. Mirabel & Rodríguez 1994, Fan, Xie & Wen 1996, Jorstad et al. 2001, Kellermann et al. 2004) and so on. This may be because jets or jet-like outflows are common among various kinds of astrophysical phenomena with different scales, such as sun, proto-stellar systems, isolated neutron stars, neutron star and black hole binaries, supermassive black holes (or AGNs) and GRBs (Zhang 2007). Once the apparent velocity is measurable, one can have opportunity to learn the geometry and the underlying physics on the formation, ejection and acceleration of jets (Ghisellini & Celotti A 2002).

AGNs are generally thought to originate from supermassive black holes located in their centers. Classification is a very important strategy to comprehend their basic physics. They can be classified into several groups or subgroups by means of some diagnostic diagrams, e.g. Seyfert I and II galaxies, Quasars, Blazars (BL lac Objects and OVV's), radio galaxies, and LINER. On the whole, Blazars, radio galaxies and part of Quasars are radio-loud, the remainder is radio-quiet. The radio-loud AGNs typically exhibit strong radio radiation, variable, jetted outflows, and X-ray emission and UV excess. This is surprisingly similar to what have been observed in GRBs. Moreover, these radio-loud sources together with GRBs have a common property that the ejecta from their cores move very close to the speed of light outwards and both of them are similarly cosmological outbursts. Till now, only two GRBs, e.g. 030329 and 170817A, are promised to have the detectably superluminal phenomenon in radio bands (Dado, Dar & De Rujula 2004, 2018; Taylor et al. 2004). Although the superluminal motions of GRBs in high energy afterglows even prompt γ -rays are invisible currently, the superluminal effect for some GRBs would do exist in theory, as long as the synergetic conditions such as viewing angles and boosting lorentz factors of outflows were satisfied (see Fig. 1). This motivates us to give a comparative study between

GRBs and radio-loud AGNs on the superluminal motion. Besides, GRBs in the pre-Swift and Swift eras have also been compared to check the dependency of the apparent transverse velocity on different instruments.

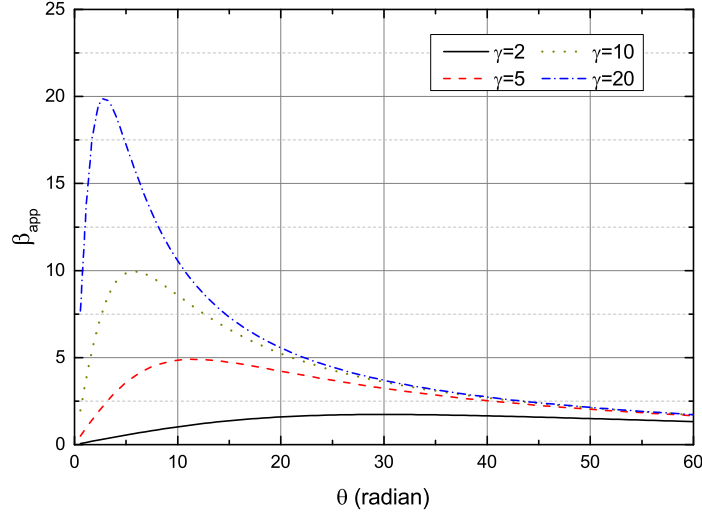


Fig. 1. The apparent transverse velocity β_{app} vs. the viewing angle θ . Note that every $\beta_{app} > 1$ corresponds a possible maximum angle $\theta_{max} = \arccos \beta$.

2. Superluminal motion

According to the relative geometry of ejecta to the observer, the apparent transverse velocity β_{app} is generally defined by

$$\beta_{app} = \frac{\beta \sin \theta}{1 - \beta \cos \theta} \quad (1)$$

in an unit of speed of light c , of which β represents the real speed of ejecta and θ is the viewing angle between the line of sight and the bulk velocity outwards. Note that the β is also in the unit of c and associated with Lorentz factor γ by $\beta = (1 - \gamma^{-2})^{0.5}$. For a given γ , one can make a plot of β_{app} versus θ , where shows a single peak profile at $\theta \approx 1/\gamma$ (Cohen, Lister & Vermeulen 2004, Kellermann et al. 2007).

In addition to β_{app} , Doppler factor δ is also connected with θ and γ as

$$\delta = \frac{1}{\gamma(1 - \beta \cos \theta)}, \quad (2)$$

In Eqs. (1) and (2), four independent variables, i.e. β_{app} , β , θ and δ , are involved. Provided two of them have been known in advance, the rest two should be deduced immediately. For the radio observations to AGNs with measured redshift (z), β_{app} is in general measurable and determined by

$$\beta_{app} = \frac{\mu D_A}{c}, \quad (3)$$

where μ is the observed proper motion in an unit of mas/yr, D_A denotes the angular diameter distance of radio source. In practice, the physical luminosity distance, D_L in the flux expression of $f = L/(4\pi D_L^2)$, is usually used for cosmological studies. D_A and D_L are tied with each other as

$$D_L = (1 + z)^2 D_A, \quad (4)$$

Hence, β_{app} can then be newly expressed as follows

$$\beta_{app} = \frac{\mu D_L}{c(1 + z)^2}, \quad (5)$$

The Doppler factor δ (Ghisellini et al. 1993) is estimated by

$$\delta = f(\alpha) S_m \left[\frac{\ln(\nu_b/\nu_m)}{S_x \phi_d^{6+4\alpha} \nu_x^\alpha \nu_m^{5+3\alpha}} \right]^{1/(4+2\alpha)} \cdot (1 + z); \quad (6)$$

where $f(\alpha) \approx 0.08\alpha + 0.14$ is an exponential function decided by an index α of the enhancement ($\propto \delta^\alpha$) of the observed flux due to beaming effect, S_m is the maximum flux at the frequency ν_m in GHz. S_x like S_m in the unit of Jansky (Jy) represents the flux within the range of any other energy band ν_x , other than the radio. ν_b and ϕ_d are the synchrotron high energy cutoff and the size of core, respectively. As for AGNs, if only the redshift can be gotten from the radio spectra one always calculate β_{app} and δ , and then β and θ .

In principle, the superluminal phenomenon can be seen as long as the viewing angle θ is suitably small enough in comparison with the opening angle $\sim 1/\gamma$ of outflows due to the beaming action. For a given source, its opening angle is generally knowable in a direct or indirect way, which makes Eq. (1) degenerate into three scenarios in the following three cases of θ as:

1. In the case of $\theta \ll \gamma^{-1}$, the observer is enveloped within the cone of jets. Some simplified forms of $\sin \theta \sim \theta$ and $\cos \theta \sim 1$ lead Eq.(1) to be rewritten as

$$\beta_{app} \approx 2\gamma^2\theta \quad (7)$$

2. In the case of $\theta \sim \gamma^{-1}$, one can just see the edge of outflows under assumption that jets do not behave a significant expanding sideways. Relations of $\cos \theta \sim 1 - \gamma^{-2}/2$, $\sin \theta \sim \gamma^{-1}$ and $\beta = 1 - \gamma^{-2}/2$ are derived. In this way, β_{app} will be reduced and reach its maximum as

$$\beta_{app} \approx \gamma \approx \delta \approx \csc \theta \quad (8)$$

3. In the case of $\theta \gg \gamma^{-1}$, the observer is located out of the cone of jets, which means $\sin \theta \sim \theta$, $\cos \theta \sim 1 - \theta^2/2$ and $\beta \sim 1$, thus

$$\beta_{app} \approx 2/\theta \quad (9)$$

3. Samples

In view of above considerations, 8 radio galaxies, 15 BL Lac objects, and 46 quasars with superluminal observations by VLBI have been chosen from literatures (Hong et al. 1995, Jorstad et al. 2001, Kellermann et al. 2004), to constitute three independent AGN samples table 1.

For GRBs, present observations of radio afterglows hiding superluminal motion are very rare. Till now, ONLY GRB 030329 and GRB 980425 are suggested to be the potential candidates (e.g. Dar & De Rujula 2000; Dado, Dar & De Rujula 2004). The reason is that the angular resolution of current antennae is still too lower to measure the proper motion of GRB afterglows, except for GRB 030329 (Taylor et al. 2004). It will be more difficult to describe the superluminal motion in the phase of prompt emissions due to lack of much higher resolution. This causes Eq.(3) to be impossible for deriving β_{app} . Alternatively, Eq. (1) can be used to investigate the superluminal motion during the prompt γ -ray emissions if only the viewing angle θ can be conveniently measured provided the Lorentz factors of GRBs are roughly estimated by

$$\gamma \approx 240 \times E_{iso,52}^{1/8} n_1^{-1/8} (T_{90}/10s)^{-3/8}, \quad (10)$$

as suggested by Rees & Mészáros (1992). Here, it has been assumed that the jet opening angle θ_j is equivalent to the viewing angle θ since the jetted outflow from us is much farther than that from its central engine, which will give the upper limits to estimate the apparent velocities of GRBs. As seen in Fig. 1, larger lorentz factors together with wider viewing angles will result in an enhancement of the superluminal motion. Based on the consideration, the apparent superluminal motion of GRBs in their prompt phase had been studied. For the sake of comparison, 27 Swift and 37 pre-Swift long GRBs with known redshift, duration time and jet break time are taken from Zhang, Zhao & Zhang (2011). In addition, I pay particular attention to GRB 170817A whose redshift, lorentz factor and viewing angle are estimated as $z = 0.0098$ (Levan et al. 2017), $\gamma \approx 13$ (Zou et al. 2018) and $30^\circ \geq \theta \geq 23^\circ$ (Haggard et al. 2017; Ioka & Nakamura 2017), respectively. Using these measured values, one can easily obtain the apparent transverse velocity of GRB 170817A to be $\beta_{app} = 4.2_{-0.4}^{+0.5}$ and the Doppler factor as $\delta = 0.74_{-0.18}^{+0.21}$.

4. Results

In this section, the main results related to superluminal motion are displayed for different kinds of cosmological sources. I pay special attention to the comparison between AGNs and GRBs in both radio and γ energy bands.

4.1. Relations of β_{app} with δ , z and γ

Fig. 2 shows a largely different population between GRBs and AGNs in the plane of β_{app} versus δ . For pre-Swift and Swift long GRBs, however, they exhibit a similar positively correlated tendency. The dotted and dashed lines correspond to their best fits to the GRB data, following a very close power-law of $\beta_{app} \sim \delta^{0.5}$. Unlike GRBs, most AGNs locate within the range of $\theta \geq 0.1\gamma^{-1}$ and roughly distribute along the line of $\beta_{app} \propto \delta$ with larger dispersion. A linear correlative analysis gives the correlation coefficient of 0.6 for all AGNs with a tiny chance probability of $P < 0.0001$.

Another interesting phenomenon seen from Fig.3 is that β_{app} obviously evolve with redshift for any kinds of these cosmological sources. Furthermore, Fig.3 shows the positive correlation of β_{app} with redshift becomes more tight when all AGNs and GRBs are combined to be a whole sample. The positive correlations demonstrate farther the sources observed larger the apparent transverse velocity. Based on the three relations between θ and $1/\gamma$ in section 2, we see that $\beta_{app} \sim \gamma$ and $\beta_{app} \sim 2/\theta$ when $\theta \sim 1/\gamma$ and $\theta > 1/\gamma$

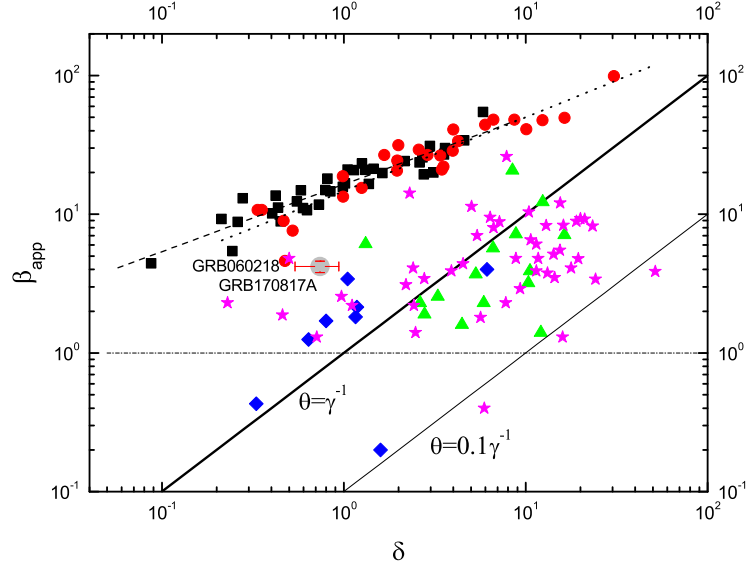


Fig. 2. The apparent transverse velocity β_{app} vs. the Doppler factor δ for AGNs and GRBs in our samples. *Circles*: Swift GRBs; *squares*: pre-Swift GRBs; *stars*: quasars; *triangles*: BL Lac objects; *diamonds*: Radio galaxies. Thick, thin and dash-dotted lines denote the relations of $\beta_{app} = \delta$, $\beta_{app} = 0.1\delta$ and $\beta_{app} = \text{constant}$, respectively. The dotted and dashed lines correspond to their best fits to the GRB data. All the symbols defined here are same to those in the Figs. 3, 4 and 5.

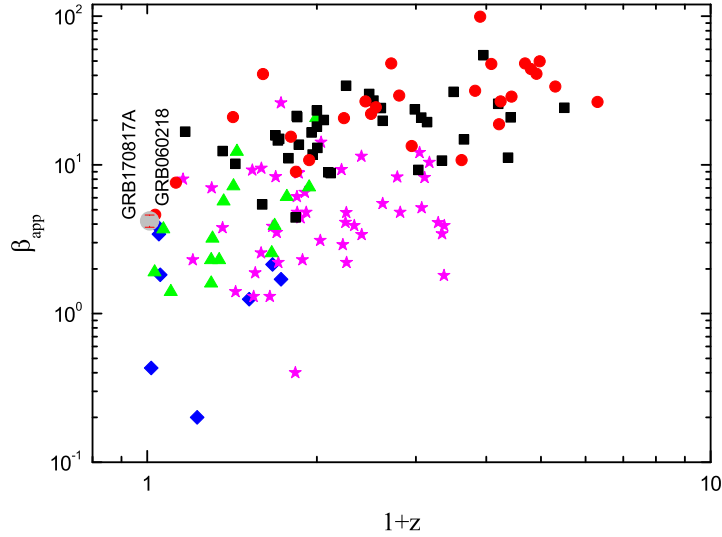


Fig. 3. The apparent transverse velocity β_{app} vs. cosmological inflation factor of $1+z$ in the logarithmic scale.

for AGNs and GRBs, respectively. γ and β_{app} are tightly correlated for the different radio-loud AGNs, while there is no any relation for LGRBs. This is because the viewing angle θ is far large than $1/\gamma$, which cause β_{app} becomes only dependent on θ . However, AGNs with $\theta \sim 1/\gamma$ seen from Fig.2 make them locate around the line of $\beta_{app} \sim \gamma$.

Plot of β_{app} vs. γ in Fig.4a shows how the apparent transverse velocity is affected by Lorentz factor for all the radio-loud AGNs and LGRBs. It is interestingly found that the β_{app} is positively correlated with γ , while this trend disappears for GRBs. Fig.4b indicates that the intrinsic observations, e.g. some typically comoving timescale in source frame, reduced for cosmological inflation and Doppler effect still hold above similar properties for different AGNs and GRBs. This means AGNs and GRBs are basically distinct cosmological sources in nature.

In addition, one can find in Figs. 2, 3 and 4 that radio galaxies are distributed in the small end of β_{app} , largely different from BL Lac objects and Quasars, much less the LGRBs. This means the radio galaxies with lower radio luminosity are very special and may thus result from a distinct origin, compared with other radio-loud AGNs such as BL Lac objects and Quasars.

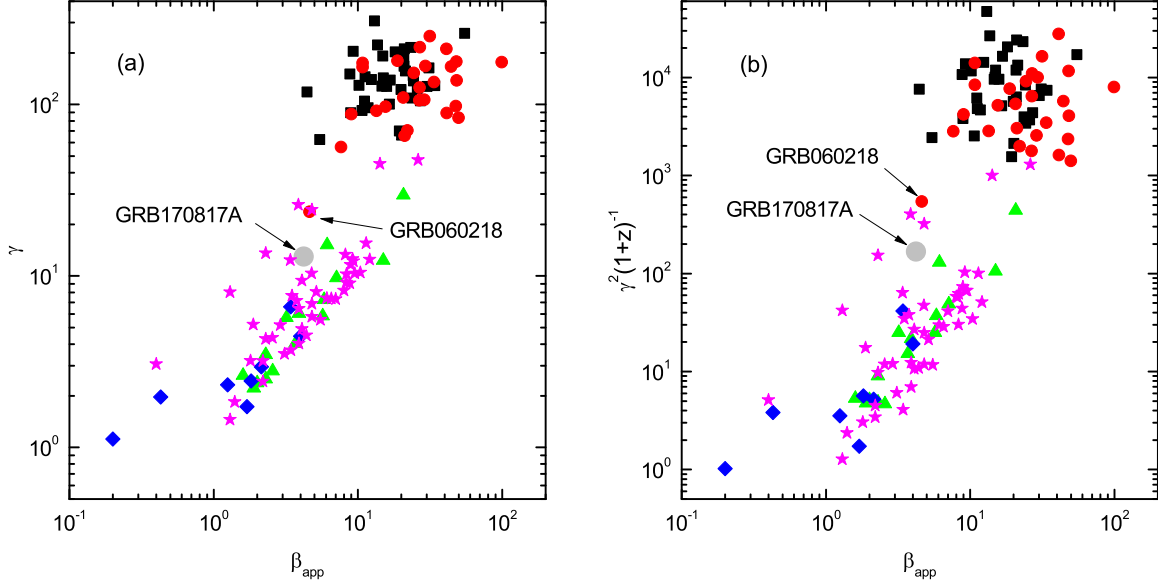


Fig. 4. Correlations of the apparent velocity β_{app} with the Lorentz factor γ in panel (a) and the modificatory factor $\gamma^2(1+z)^{-1}$ for the effects of Doppler boosting and cosmological expansion in panel (b), respectively.

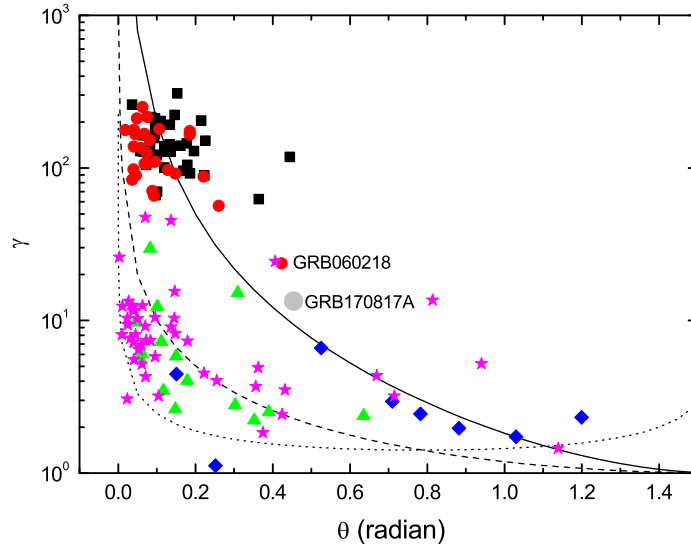


Fig. 5. The Lorentz factor γ vs. the viewing angle θ . *Solid line* corresponds to $\delta = 1$; *dashed line* represents $\gamma = 1/\sin\theta$; and *dotted line* describes $\beta_{app} = 1$.

4.2. Correlation between γ and θ

In Fig.5, we compare these sources in the γ vs. θ plane. The top-right region of $\delta = 1$ corresponds to $\delta < 1$ and the reverse direction is within the range of $\delta > 1$. Similarly, the bottom-left of $\beta_{app} = 1$ represents $\beta_{app} < 1$ and the top-right of $\beta_{app} = 1$ stands for $\beta_{app} > 1$. Very clearly, most of AGNs and GRBs reside between the solid line and the dotted one, in the area of $\beta_{app} > 1$ and $\delta > 1$. The result on AGNs is extremely consistent with that suggested by Ghisellini (1993) in theory. But we again find the radio galaxies with lower lorentz factor compared to other AGNs locate at the larger end of θ . Another interesting phenomenon is GRBs with smaller viewing angle distribute at the larger end of γ . This indicates that the beaming effect could be really not very important for the radio galaxies, unlike for GRBs, BL Lac objects and Quasars. A majority of AGNs follows $\gamma = 1/\sin\theta$, that is $\beta_{app} = \beta\delta$, while GRBs cluster along the line of $\delta = 1$. In fact, the locations of GRBs might move towards the short end of θ slightly if the jet evolution is considered.

4.3. Violators

It is well-known that GRB 060218 is a typical low luminosity burst ($T_{90} \sim 2100s$) connected with SN 2006aj, a supernovae Ib/c (e.g. Mirabal et al. 2006; Li 2007). Recently, Zhang et al. (2018a) noticed that GRB 060218, together with 980425 and 031203, deviated from the normal evolution curves of long bursts in the plane of peak flux density versus redshift at different radio frequencies. GRB 170817A is a peculiarly newly-discovered short GRB ($T_{90} \sim 2s$) associated with gravitational wave (GW), which was reported as the first electromagnetic counterpart of a GW event originated from binary Neutron stars (Abbott et al. 2016a,b). With more and more short bursts accumulated with redshift and peak energy, their spectrum-energy relations can be built as long bursts did before. Excitingly, three spectrum-energy correlations have been proposed by Zhang et al. (2018b) and the GRB 170817A, unlike other short and long bursts, is identified as an outlier to all the three energy relations of short GRBs. It is interesting to note here that GRB 170817A is also found to be very different from long bursts but similar to GRB 060218 regarding the superluminal motion. This may hint that those low luminosity GRBs could hold the consistent observations related with the superluminal motions.

5. Conclusions and discussions

Our main results are summarized and concluded in the following:

1. The apparent transverse velocity β_{app} is found to be correlated with δ as $\beta_{app} \propto \delta$ for LGRBs and $\beta_{app} \propto \delta^{0.5}$ for radio-loud AGNs.
2. Radio galaxies are special AGNs with lower redshift, luminosity, γ and δ , which makes it a very different radio-loud sources.
3. Figs. 2,4 and 5 seem to demonstrate GRBs and AGNs may have different radiation mechanisms and Doppler (or beaming) effect. However, their cosmological evolution might be same as shown in Fig. 3 in respect of the superluminal motion.
4. As low luminosity GRBs, 060218 and 170817A are obvious violators to the above relation of both long GRBs and three types of AGNs and have very similar behaviors although they are largely different in duration time T_{90} .

As suggested by Kellermann et al. (2004), radio jets that are also strong gamma-ray sources detected by EGRET appear to have significantly faster speeds than non-EGRET sources, which is much consistent with the idea that gamma-ray sources have larger Doppler factors than non-Cgamma-ray sources. Kellermann et al. (2004) also pointed that there is a systematic decrease in apparent velocity with increasing wavelength, probably because the observations at different wavelengths sample built from different parts of the jet structure. It is required to test whether this is also true for GRBs because the current sample with with superluminal motion for GRB radio afterglows are very limited, ONLY GRB 030329 and possibly GRB 980425. In such a case, observational investigations on superluminal motion of GRBs are particularly expected in the near future.

The typically extragalactic sources with high redshift are usually useful for studying the formation and evolution of the early universe. So far, the farthest galaxy is found to have a spectroscopic redshift of $z = 6.96$ (Iye et al. 2006). Fan et al. (2001) found the most distant AGN was Quasar SDSS J1030+0524 with a redshift of $z = 6.28$, which was taken among follow-up spectroscopy of i-band drop-out objects. Cosmological GRBs are the ideal candidates for the universal study since several GRBs have been found to locate at very high universe with redshifts larger than $z \sim 6$, e.g., GRB 080913 ($z = 6.7$, Greiner, J. et al. 2009), GRB 050904 ($z = 6.39$, Haislip et al. 2006) and GRB090423 ($z = 8.1$, Salvaterra et al. 2009). In principle, superluminal motions should be detectable and similar for all the distant celestial bodies if only the true velocity of the outflow is close to the speed of light and the viewing angle θ is sufficiently small, due to the beaming effect of special relativity (see also Zhang et al. 2007). In addition, this phenomenon would be multiple-band observed if the receiver on ground is sensitive enough. However, studies on superluminal motions of these sources proceed slowly till now owing to the lack of radio observations with high resolution.

In statistics, roughly 15-20% of AGNs are radio-loud. The variability of radio-loud AGNs behaves much active over wide wavelengths (Xie et al. 1994). Unlike the steep-spectrum for radio-quiet AGNs, the spectrum of radio-loud AGNs is generally flat because of the more beamed outflows at radio frequencies, but not in the optical and X-ray energy bands. This might imply that radio-loud AGNs are jet-dominated at radio frequencies and disk-dominated in the X-ray and optical band. Even though, the radio mechanism of the radio-loud AGNs could be very different from that of LGRBs. The later with a single or double power-law form is thought to be basically produced from the processes of synchrotron radiation and inverse-Compton scattering. Currently, the real radiation mechanism of AGNs and GRBs are still not confirmed and needs to be further clarified.

Acknowledgements. This work is supported by the National Natural Science Foundation of China (grant number: U1431126, 11263002), Guizhou natural and scientific fundings (grant numbers: 20165660, 201519, OP201511 and 114A11KYSB20160008).

References

- Abbott, B. P., Abbott, R., Abbott, T. et al., 2016a, PhRvL, 116, 241103
 Abbott, B. P., Abbott, R., Abbott, T. D. et al., 2016b, PhRvD, 93, 122003
 Chodorowski, Michal J., 2005, AmJPh, 73, 639
 Cohen, M. H., et al. 1971, ApJ, 170, 207
 Cohen, M. H., Lister, M. L., Vermeulen, R. C., 2005, EAS, 15, 93. astro-ph/0402158v1
 Dado, s., Dar, A., & De Rujula, A., astro-ph/0008474
 Dado, S., Dar, A. & De Rujula, A., astro-ph/0402374
 Dado, S., Dar, A. & De Rujula, A., astro-ph/1712.09970
 Fan, J. H., Xie, G. Z., & Wen, S. L. 1996, A&AS, 116, 409
 Fan, J. H., Wang, Y. J., Yang, J. H., & Su, C. Y. 2004, ChJAA, 4, 533
 Fan, x. H. 2001, AJ, 122, 2833
 Levan, A. J., Lyman, J. D., Tanvir, N. R., et al. 2017, ApJ, 848, L28

- Li, Li-Xin, 2007, MNRAS, 375, 240
Mirabal, N.; Halpern, J. P.; An, D., et al., 2006, ApJ, 643, L99
Ghisellini, G. 1993, ApJ, 407, 65
Ghisellini G., & Celotti A., astro-ph/0204333v1
Greiner, J., et al. 2009, ApJ, 693, 1610
Haislip J. B., et al. 2006, Nature, 440, 181
Hong, X. Y., Jiang, D. R., & Wan, T. S. 1995, ACTA ASTRONOMICA SINICA, 36, 147
Haggard, Daryl; Nynka, Melania; Ruan, John J.; et al., 2017, ApJ, 848, L25
Iye, M., et al. 2006, Nature 443, 186
Ioka, Kunihito; Nakamura, Takashi, 2017, arXiv171005905I
Jorstad S. G., Marscher A. P., Mattox J. R., et al. 2001, ApJS, 134, 181
Kellermann K. I., Lister M. L., Homan D. C. et al. 2004, ApJ, 609, 539
Kellermann K. I., et al. 2007, Ap&SS, 311, 231
Mirabel, I. F. & Rodríguez, L. F. 1994, Nature, 371, 46
Rees, M. J. 1966, Nature, 211, 468
Rees, M. J. & Mészáros, P., 1992, MNRAS, 258, 41
Salvatterra et al. 2009, Nature, 461, 1258
Taylor, G. B., Frail, D. A., Berger, E., Kulkarni, S. R., 2004, ApJ, 609, L1
Whitney, Alan R., et al. 1971, Science, 173, 225
Xie G. Z., Li K. H., Zhang Y. H. et al. 1994, A&AS, 106, 361
Zhang, S. N., HiA, 14, 41. astro-ph/0702246v3
Zhang, Z. B., Zhao, Y.X., Zhang, Y.Z., 2011, Ap&SS.333, 89
Zhang, Z. B.; Chandra, P.; Huang, Y. F.; Li, D., 2018a, submitted to ApJS, arXiv180100397.
Zhang, Z. B.; Zhang, C.T.; Zhao, Y. X. et al., 2018b, accepted by PASP.
Zou, Y.-C., Wang, F.-F., Moharana, R., et al., 2018, ApJ, 852, L1

Table 1. Samples of Radio-Loud AGNs (B: Blazars; G: radio Galaxies; Q: Quassars)

IAU	type	z	β_{app}	θ	δ	γ	β
1219+285	B	0.102	2	36.41	1.56	2.38	0.90745
0219+428	B	0.444	14.98	5.8	1.99	12.34	0.99671
0235+164	B	0.94	7.1	2.57	16.32	9.74	0.99472
0454+844	B	0.3	1.6	8.49	4.46	2.63	0.92489
0716+714	B	0.3	2.3	22.33	2.63	2.51	0.91721
0735+178	B	0.424	5.84	6.39	3.17	7.27	0.99049
0851+202	B	0.306	3.2	3.16	10.33	5.71	0.98455
0954+658	B	0.367	5.7	8.61	6.62	5.84	0.98523
1101+384	B	0.031	1.9	20.2	2.78	2.22	0.8928
1308+326	B	0.996	20.7	4.74	8.45	29.65	0.99943
1749+701	B	0.77	6.12	17.76	1.32	15.18	0.99783
1803+784	B	0.684	3.9	3.56	10.55	6.04	0.9862
1823+568	B	0.664	2.56	17.35	3.29	2.79	0.93356
2007+776	B	0.342	2.3	6.73	5.89	3.48	0.95782
2200+420	B	0.069	3.7	10.24	5.32	4.04	0.96888
1323+321	G	0.729	1.7	59	0.8	1.73	0.81601
0108+388	G	0.669	2.14	40.66	1.18	2.95	0.94079
0710+439	G	0.518	1.25	68.73	0.64	2.32	0.90234
1845+797	G	0.0546	1.82	44.83	1.16	2.44	0.91216
2021+614	G	0.227	0.2	14.42	1.59	1.12	0.45034
0430+052	G	0.033	4	8.65	6.13	4.45	0.97442
0316+413	G	0.017	0.43	50.54	0.33	1.97	0.86158
0415+379	G	0.049	3.42	30.12	1.05	6.6	0.98845
1830+285	Q	0.594	2.55	38.36	0.97	4.35	0.97322
2223-052	Q	1.404	3.4	0.65	24.24	12.38	0.99673
1721+343	Q	0.206	2.3	46.64	0.23	13.6	0.99729
1253-055	Q	0.538	9.2	1.99	21.09	12.58	0.99684
1226+023	Q	0.158	8	8.48	6.66	8.21	0.99255
2230+114	Q	1.037	14.2	7.85	2.3	45.13	0.99975
1222+216	Q	0.435	1.4	21.49	2.48	1.84	0.83942
1828+487	Q	0.691	8.32	2.9	16.14	10.25	0.99523
1458+718	Q	0.905	6.53	4.79	10.68	7.38	0.99078
1633+382	Q	1.814	4.8	5.48	8.83	5.78	0.98492
1641+399	Q	0.595	9.5	8.32	6.37	10.35	0.99532
1618+177	Q	0.555	1.88	53.9	0.46	5.21	0.98141
1928+738	Q	0.302	7	10.29	5.4	7.33	0.99065
1611+343	Q	1.401	11.4	8.4	5.04	15.52	0.99792
1510-089*	Q	0.361	3.77	2.31	13.18	7.17	0.99023
1606+106*	Q	1.226	2.9	3.52	9.32	5.16	0.98104
1156+295	Q	0.729	26.1	4.03	7.85	47.38	0.99978
1150+812	Q	1.25	4.1	20.77	2.41	4.9	0.97895
1137+660	Q	0.652	1.3	65.29	0.71	1.45	0.72414
0420-00	Q	0.844	6.1	4.17	11.46	7.4	0.99083
0420-014*	Q	0.915	4.8	3.45	11.72	6.89	0.98941
0458-020*	Q	2.286	4.09	1.41	17.8	9.4	0.99433
0528+134	Q	2.07	5.15	2.59	14.22	8.08	0.99231
0538+498	Q	0.545	1.3	0.58	15.94	8.05	0.99225
0336-01	Q	0.852	8.9	2.32	19.01	11.61	0.99628
0333+321	Q	1.258	4.77	1.37	19.45	10.34	0.99531
0106+013	Q	2.107	8.2	1.54	23.34	13.34	0.99719
0153+744	Q	2.34	3.43	20.41	2.77	3.69	0.96258
0202+149	Q	0.833	0.4	1.34	5.93	3.06	0.94509
0212+735	Q	2.37	3.9	3.07	11.46	6.44	0.98787
0234+285	Q	1.213	9.29	2.19	19.99	12.18	0.99662
0552+398	Q	2.365	1.8	6.02	5.65	3.2	0.94992
0605-08*	Q	0.872	4.4	12.75	4.53	4.51	0.97511
0923+392	Q	0.699	3.5	1.83	14.42	7.67	0.99146
0016+731	Q	1.781	8.3	4.03	12.95	9.17	0.99404
1039+811	Q	1.26	2.2	40.99	1.11	3.19	0.94959
1040+123	Q	1.029	3.1	24.76	2.2	3.51	0.95856
1055+018*	Q	0.888	2.3	4.06	7.78	4.29	0.97245
0906+430	Q	0.67	3.86	0.17	51.64	25.97	0.99926
0850+581	Q	1.332	3.9	14.63	3.9	4.03	0.96872
0615+820	Q	0.71	2.2	24.3	2.43	2.42	0.91063
0711+356	Q	1.62	5.5	2.36	15.41	5.54	0.98357
0723+679	Q	0.846	4.8	23.3	0.5	24.35	0.99916
0827+243	Q	2.046	12.08	3.6	15.46	12.48	0.99678
0836+710	Q	2.17	10.4	5.51	10.41	10.45	0.99541
2251+158	Q	0.859	8.8	7.83	7.18	9.05	0.99388